Dyes and Pigments 175 (2020) 108129

Contents lists available at ScienceDirect

Dyes and Pigments

journal homepage: http://www.elsevier.com/locate/dyepig

A new method to synthesize Sub-10 nm CaF_2: Nd^{3+} nanoparticles and fluorescent enhancement via Li^+ ions or Ce^{3+} ions doping

Tan Wang [a,b,c], Yaguo Yu [a], Xiaonan Ji [a,c], Wei Xu [a], Yanyan Fu [a], Huimin Cao [a], Qingguo He [a,*], Jiangong Cheng [a,**]

[a] State Key Lab of Transducer Technology, Shanghai Institute of Microsystem and Information Technology, Chinese Academy of Sciences, Changning Road 865, Shanghai, 200050, China
[b] School of Physical Science and Technology, ShanghaiTech University, 201210, Shanghai, China
[c] University of the Chinese Academy of Sciences, Yuquan Road 19, Beijing, 100039, China

ARTICLE INFO

Keywords:
CaF_2 nanoparticles
Coprecipitation
Lanthanide doping
Fluorescence

ABSTRACT

In this contribution, we provided a new, simple, cheap, repeatable and easily tunable method to synthesize CaF_2: Nd^{3+} NPs using coprecipitation strategy. By controlling reaction time, temperature and solute/solvent, CaF_2: Nd^{3+} NPs with dimeters ranging from 2.2–4.6 nm were synthesized. Then we optimized the Nd^{3+} concentration and found CaF_2:6Nd(mol%) NPs with strongest luminescence. Furthermore, to further enhance the fluorescence of the optimized NPs, we explored both Li^+ doping and Ce^{3+} doping to afford highly fluorescent CaF_2:Nd^{3+} NPs. For Li^+ doping CaF_2:6Nd,xLi(mol%) NPs, under the excitation of 800 nm, a ~4-fold fluorescence enhancement was observed, while for Ce^{3+} doping CaF_2:6Nd,xCe(mol%) NPs, a 10.4-fold fluorescence enhancement was observed. Li^+ doping leads to two fluorescence maxima at 4% and 30%, mainly dominated by charge compensation, and increased crystallity/grain size, separately. As comparison, Ce^{3+} doping resulted in the monotonical increase of the fluorescence, dominated by lowered crystal symmetry, changed local crystal field and dissociated Nd^{3+} - Nd^{3+} clusters.

1. Introduction

During the past few years, lanthanide (Ln) nanoparticles (NPs) with efficient frequency conversion from NIR to NIR radiation in luminescent materials have arisen great concern in potential for many applications such as bioimaging, displays, phototherapy and photocatalysis, due to their narrow emission peak, large Stokes shift, good chemical and physical stability, low toxicity, low tissue heat damage and high spatiotemporal resolution [1–3]. The commonly NIR fluorescence ignited from Ln^{3+} doped NPs has been systematically summed up [4–6]. Comparing Yb^{3+} activated NPs emitting at NIR-II which are excited with 980 nm lamp where water absorption is so strong, Nd^{3+} doped NPs has strong absorption band around 800 nm (where water absorption is so weak), narrow FWHM of emission peak, superior efficient downshifting (DS) [7] and emission band around 1.0–1.35 μm [8]. Considering these advantages, we chose Nd^{3+} doped NPs to achieve highly efficient NIR-fluorescent material. What's more, like other lanthanide-based host materials such as LnF_3 or $ALnF_4$ (where A = Li, Na, K), CaF_2 is a charming host for phosphors with interesting up/down-conversion luminescent properties [9]. The edge of the fundamental absorption band in CaF_2 lies in the vacuum UV at ~ 12 eV [10,11]. Finally, CaF_2 has a well-known fluorite structure, in which Ca^{2+} ions lie at the nodes in a face-centered lattice, while F^- ones lie at the centers of the octants, the Ca^{2+} ion can be easily substituted by a trivalent lanthanide ion because of similarity in ionic radius [12]; charge compensation can easily be achieved by defect formation [13].

Up to now, methods of synthesizing lanthanide-based NPs have been widely reported, including thermal decomposition, thermal coprecipitation, hydro/solvothermal, combustion, microwave, and so on [14]. Especially for CaF_2:Ln^{3+} NPs, most of the synthesis were conducted by thermal decomposition [15] and hydro/solvothermal [16], these explorations have contributed a lot for the later research in this area. Although decomposition method is easy for size control, trifluoroacetic acid has to be used to get calcium trifluoroacetate, which is complex and damages repeatability. Hydro/solvothermal way is easy to conduct, however hard to observe the reaction process and control the size of the

* Corresponding author.
** Corresponding author.
E-mail addresses: hqg@mail.sim.ac.cn (Q. He), jgcheng@mail.sim.ac.cn (J. Cheng).

https://doi.org/10.1016/j.dyepig.2019.108129
Received 15 November 2019; Received in revised form 9 December 2019; Accepted 10 December 2019
Available online 11 December 2019

NPs. Herein, a simple, cheap, repeatable and easily tunable method was proposed. Thermal coprecipitation has been widely used to synthesize $ALnF_4$ (where A = Li, Na, K) [17], but it hasn't been used for the synthesis of CaF_2 NPs, we hope to utilize it to synthesize CaF_2 NPs. Instead of using calcium trifluoroacetate to produce CaF_2 NPs, we dissolved Ca $(OH)_2$ and lanthanide acetate into OA (Oleic acid) and ODE (1-Octadecene) mixture to get Ca(Ln)-OA-ODE precursor firstly, then removed heating and cooled to room temperature, poured into the methanol solution of NH_4F, at last heated to ~ 300 °C and centrifuged to afford the CaF_2 NPs. There are three merits for our method. Firstly, it enjoys high experimental repeatability. Mainly because NH_4F was added to a neural condition to afford CaF_2, which avoided the decomposition of NH_4F in either too acidic or too alkalic environment. Secondly, it is easy to control the process, such as modulating A: Ln: F [18], reaction time [19,20], M: OA: ODE(M claims metal ions, including A and Ln) [21], temperature [22], dopant concentration [23] and stirring [24,25] et al. Thirdly, it is time-efficient, there is no residual immediate process and the final reaction under ~300 °C is ~60 min. Finally, the chemical reagents for the synthesis are commercially available and cheaper compared with calcium trifluoroacetate method.

Subsequently, we studied the effects of dopant concentration of Li^+ ions and Ce^{3+} ions to modify the material to attain stronger fluorescence. For Li^+ ions doping, it has been thought to be very effective in enhancing fluorescence by improving crystallinity [26], grain size [26], surface roughness [27], charge compensation [28], and increasing in lifetime of intermediate levels [29]. What's more, Li^+ has a distinguished charge and diameter (Li^+ is 0.76 Å, Ca^{2+} is 1.0 Å) property from Ca^{2+}. We investigated Li^+ doping effect and found that there are two luminescent maxima at Li^+ dopant concentrations of 4% and 30%. Maximum at 4% was mainly resulted from charge compensation, while that at 30% was mainly originated from improved crystallinity and increased grain size.

Finally, Ce^{3+} doping has been widely used in Yb^{3+}-Er^{3+} to weaken the up-conversion and inversely increase the wanted down-conversion by phonon-assisted energy transfer mechanism [30] or functioned in Ce^{3+}-Nd^{3+} as more effective sensitizer [31]. Ce^{3+} ion has distinguished charge and diameter (Li^+ is 0.76 Å, Ce^{3+} is 1.02 Å, Ca^{2+} is 1.0 Å) from Ca^{2+} and Li^+, but coordinated to Nd^{3+}(0.98 Å). So we further investigated Ce^{3+} effect on the fluorescence of the NPs and found CaF_2:6Nd, xCe(mol%) NPs showed a different mechanism and a much stronger fluorescence than Li^+ doping case.

2. Experimental

2.1. Materials and methods

All chemicals were used as received without any further purification. $Nd(CH_3CO_2)_3{\cdot}4H_2O$ (99.99%), $Ce(CH_3CO_2)_3{\cdot}xH_2O$ (x = 1 ~ 3, 99.99%), $LiOH{\cdot}H_2O$ (AR, 99%),$Ca(OH)_2$ (GR, 98%), NH_4F (99.99%), 1-Octadecene (ODE, GC, >90%), all these reagents were bought from Maclin reagent company. Oleic acid (OA, technical grade, 90%) bought from Sigma-Aldrich. Methanol (reagent grade), ethanol (reagent grade), cyclohexane (HPLC, >99.99%), were bought from Aladin reagent company.)

2.2. Synthesize CaF_2: 6Nd(mol%) NPs

1| At room temperature, calculated $Nd(CH_3CO_2)_3{\cdot}4H_2O$ (x mmol), Ca $(OH)_2$ (1-x mmol), OA (oleic acid, 8.0 mL) and ODE (1-octadecene, 12.0 mL) were mixed together in a 250 mL flask.

! Caution After the addition of $Ca(OH)_2$ into a three-necked flask, 3–5 mL ODE was dropped into it first, then flask was shaken so the powder can be fully infiltrated by the ODE, at last OA and the left ODE was poured into the mixture. (Once pouring all the solvents all together at first, some powder may float on the surface of the solvent system and difficult for a complete reaction).

2| Fit the flask with a thermocouple temperature sensor, heat the solution to 70 °C and keep for 10 min, then heated up and kept at 150 °C for 20 min under vacuum and stirring. Then the solution was cooled down to room temperature.

! Caution By our tests, keeping at 70 °C for 10 min is because the Ca $(OH)_2$ doesn't resolve well in the solvents at temperature below 70 °C, by doing so, $Ca(OH)_2$ can be well dissolved. Once it is higher than 80 °C, if there is too much undissolved $Ca(OH)_2$, there will be too many bubbles and can be sucked into the vacuum pump and cause the loss of the chemicals.

3| At room temperature, 8 mL of NH_4F-methanol stock solution was dropped into the above flask under vigorous stirring.

4| Seal the flask and heated to 40 °C under vacuum and stirring, keep the reaction at this temperature for 30 min.

5| Under a gentle argon flow, the temperature was raised to 300 °C at a heating rate of 15 °C/min. When the temperature rises to 250 °C, stop stirring. Keep the reaction mixture at 300 °C without stirring for 90 min.

6| The solution was cooled down to room temperature, centrifuged and washed twice. The nanoparticles were finally dispersed in 10 mL of cyclohexane for further use.

2.3. Synthesize CaF_2:6Nd,xLi(mol%) or CaF_2:6Nd,yCe(mol%) NPs

The synthesis of the CaF_2:6Nd,xLi(mol%) or CaF_2:6Nd,yCe(mol%) NPs were similar as that of the CaF_2: 6Nd(%) NPs, except adding the correspondent substance of $LiOH{\bullet}H_2O$ (x mmol), $Nd(CH_3CO_2)_3{\cdot}4H_2O$ (0.06 mmol), $Ca(OH)_2$ (0.94-x mmol) for CaF_2:6Nd,xLi(mol%) NPs and adding correspondent substance of $Ce(CH_3CO_2)_3{\cdot}xH_2O$(y mmol), Nd $(CH_3CO_2)_3{\cdot}4H_2O$ (0.06 mmol), $Ca(OH)_2$ (0.94-y mmol) for CaF_2:6Nd, yCe(mol%) NPs.

2.4. Characterization methods

X-ray diffraction (XRD) patterns with a resolution of 0.02° (2θ) and a scan speed of 10°/min, were collected using a Rigaku D/max 2550V diffractometer with a Cu source operating at 40 kV and 450 mA. Transmission electron microscopy (TEM) images were obtained from a JEM-2100F microscope operating at 80 kV and High-resolution (HR-TEM) images from FEI Tecnai field-emission scanning transmission electron microscope operating at 200 KV. Cyclohexane dispersions of the NCs were drop casted on a formvar carbon-coated grid (300 mesh Cu) and air-dried before imaging. Size analysis of NCs from the images were obtained by measuring at least 100 particles and averaged. Energy-dispersive X-ray spectrometer (EDS) analysis was performed during TEM measurements. Absorption spectra were collected by using a PerkinElmer Lambda 950 UV–visible–NIR spectrometer with a 5 nm step. The emission spectra were obtained on an Edinburgh Instruments FLS1000 fluorescence spectrometer equipped with an 808 nm laser as the excitation source.

3. Results and discussion

3.1. Characterization for CaF_2 NPs

To prepare CaF_2, we choose $Ca(OH)_2$ as starting material. Since it can't be easily soluble either in water or alcohols as AOH (A = Li, Na, K), CaF_2 can't be synthesized as $ALnF_4$ NPs by coprecipitation method [32]. However, we found it could be easily dissolved in OA and ODE solvents as the temperature is higher than 70 °C and concentration of $Ca(OH)_2$ is lower than 0.1 M (in our solvent system, molar ratio OA to ODE = 2:3) under stirring. After $Ca(OH)_2$ and neodymium acetate were dissolved in

the solvent system, then 2.5 equivalent methanol solution of NH_4F was added and the temperature was elevated to ~ 300 °C and held for ~60 min to afford the CaF_2:Nd^{3+} NPs.

A systematic regulation of temperature, reaction time, solute concentration and stirring was conducted to tune the size of the CaF_2:Nd^{3+} NPs.

Firstly, the reaction temperature and time was tuned, which has been widely acknowledged as the most fundamental factors in size control of nanoparticles [33]. When temperature arises, the crystal free energy and the total free energy of a nanoparticle drops down, thus the nucleation formation and the size of the NPs will be changed [34]. We set the constant experimental conditions as: Nd^{3+} 0.05 mmol, Ca^{2+} 0.95 mmol, M: (OA + ODE) = 1:20, stop stirring at 250 °C. Elevating the temperature to 250 ~ 300 °C at a rate of 20 °C/min, and held for 30 ~ 90 min. Five kinds of NPs were obtained with the reaction temperature and time change. XRD spectra in Fig. 1F and EDS spectrum in Fig. S1 depicted that our synthesized NPs is CaF_2:Nd^{3+}. Fig. 1 A ~ E showed the diameters of as synthesized CaF_2 NPs increased from ~2.2 nm to ~4.6 nm with reaction time extension and temperature enhancement. The XRD spectra in Fig. 1F (the residual XRD spectra were shown in Fig. S1) and the analysis data (Table S1) exhibited that, the higher the temperature and the longer the reaction time, the stronger comparison of the peak intensity between ~47.00° and ~28.266° (2θ degree), along with the narrowed full width at half maxima (FWHW) for the two main diffraction peaks. These results are correspondent with Ostwald ripening: namely, the small NPs dissolve, and the big ones grow even bigger [34]. As temperature and reaction time rises, the smaller NPs is easier to deposit onto the surface of bigger NPs, so the concentration of free monomers in solution is less and the reaction is more thoroughly. Therefore, by regulating reaction temperature and reaction time, the NPs' size could be successfully controlled from ~2.2 nm to ~4.6 nm.

3.2. Optical properties

Then we changed the ratio of M: (OA + ODE) and stirring for the control tests of CaF_2 NPs (supporting information Fig. S2, S3), and found that, M: (OA + ODE) = 1:20, stop stirring at 250 °C and react at 300 °C for 90 min, are the superior condition for CaF_2:Nd^{3+} NPs of 4.6 nm.

With the optimized condition of 4.6 nm NPs as basis, the CaF_2:xNd^{3+}(mol %) NPs were further prepared by a systematic tuning of the Nd^{3+} dopant concertation from 1% to 10%. The absorption spectra of CaF_2:xNd^{3+}(mol %) NPs with different Nd^{3+} dopant concentration was given in Fig. S4(Supporting Information). It could be seen that the main absorption peak is located at ~800 nm, and with Nd^{3+} doping density increasing, the absorbance grows correspondingly. Fig. 2 showed the fluorescent spectra of the NPs. As indicated, the CaF_2 NPs with 6%Nd^{3+} exhibited the strongest fluorescence with NIR emission peak at 1.06 μm. A higher or lower dopant concentration leads to a much lower fluorescence.

3.3. Li^+ doping characterization and fluorescent performances

Thirdly, we exploited Li^+ doping effect to further enhance the fluorescence of CaF_2:6Nd(mol%) NPs as mentioned above that it is very effective in enhancing fluorescence by improving crystallinity, grain size, surface roughness et al. The XRD spectra and TEM images for various Li^+-doped CaF_2:xLi,6Nd(mol%) were shown in Fig. 3. In Fig. 3A, we can see as the Li^+-doping density increase, the main diffraction peaks at 28°, 47°, 55°, 68.7°, 75.8° shifted to smaller degree (especially, the peak CaF_2:30Li,6Nd(mol%) at peak 47° decreased up to 0.64° compared with CaF_2:6Nd, Fig. S5). Moreover, the characteristic peaks for LiF at 38.7°, 45.0°, 65.5° appeared gradually and got stronger when Li^+-doping was more than 30%. What's more, there is a tendency that the FWHM at diffraction peak of 47.0° monotonously reduced from 2.1 to 0.91 with Li^+-doping from 0% to 30% (Fig. S5), nevertheless the FWHM reversely increased to 1.07 when Li^+-doping was 50%. The increased intensity of diffraction peaks and lower FWHM showed the improved crystallinity and increased grain size [35,36]. These results were consistent with Fig. 3B-E, the sizes of Li^+-doping from 0% to 30% complied with nearly monotonous size increase of the NPs from 4.59 nm

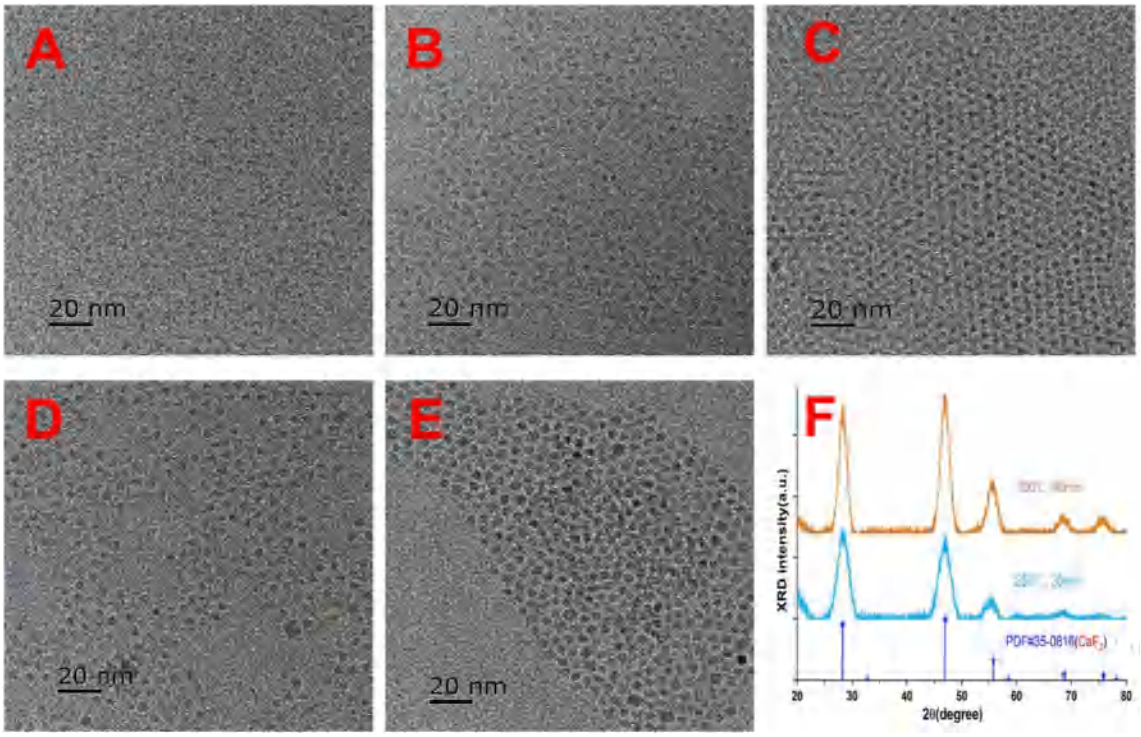

Fig. 1. **(A)** The TEM image with 20 nm scale bar for CaF_2: 5Nd(mol%) NPs reacted at 250 °C for 30 min, the size is 2.2 nm. Similarly, **(B)** the size is 3.03 nm, reacted at 280 °C for 60 min, **(C)** the size is 3.24 nm, reacted at 300 °C for 30min, **(D)** the size is 4.13 nm, reacted at 300 °C for 60 min, **(E)** the size is 4.59 nm, reacted at 300 °C for 90 min. **(F)** XRD spectra for CaF_2: Nd^{3+} NPs under different reaction conditions.

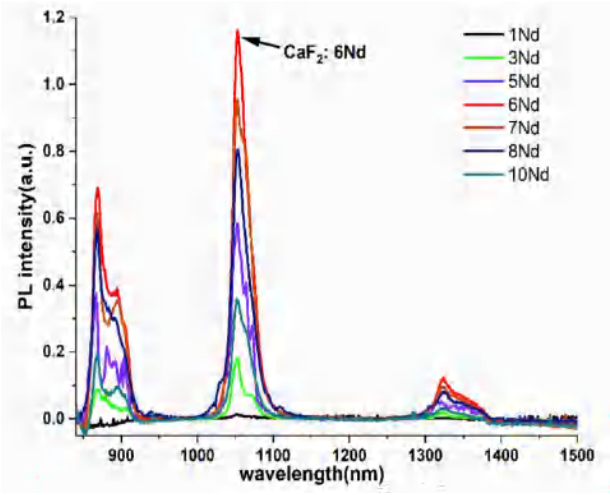

Fig. 2. The fluorescent spectrum of CaF_2:xNd(mol %) NPs around 5 nm diameter with different Nd^{3+} dopant concentration, CaF_2: 6Nd(mol %) NPs enjoys strongest intensity. All tests were in cyclohexane under 808 nm laser excitation.

(Fig. 1F) to 10.66 nm, but it reversely reduced to 7.94 nm when Li^+ density was 50%. These facts indicated that Li^+-doping could both improve the crystallinity and increase the grain size of the as-synthesized NPs.

We explored photoluminescence behavior of CaF_2:xLi,6Nd(mol%) NPs under the excitation by 808 nm laser (Fig. 4). There were two maximum values at Li^+ doping concentrations of 4% and 30%. For the intensity maxima at Li^+ doping 4%, which was 2.4 times strong than that of no Li^+ doping NPs (Fig. 4B). We thought it was mainly stemmed from charge compensation, which could be explained by the defect reactions as following equations [36,37]:

$$2NdF_3 \rightarrow 2Nd^{\bullet}_{Ca} + V''_{Ca} + 6F_F\times \quad (1)$$

$$NdF_3 + LiF \rightarrow Nd^{\bullet}_{Ca} + Li'_{Ca} + 4F_F\times \quad (2)$$

$$Nd^{\bullet}_{Ca} + Li'_{Ca} \rightarrow (Nd^{\bullet}_{Ca}Li'_{Ca}) \quad (3)$$

With increasing concentration of Nd^{3+} ion doping (there were no Li^+ ions doped), Nd^{3+} ions had been incorporated into the CaF_2 crystal lattice, which may induce structural defect $Nd^{\bullet}_{Ca}$. On the other hand, because of the difference in the valence of Nd^{3+} and Ca^{2+}, the introduction of Nd^{3+} ions into CaF_2 NPs should lead to the appearance of Ca vacancy to compensate for the charge, which can be described as Eq. (1), $2Nd^{3+}$ replace $3Ca^{2+}$ and $2Nd^{\bullet}_{Ca}$, 1Ca''(negative vacancy) is left. With Li^+-doping increasing, the incorporation of Li^+ ions can form Li'_{Ca}, which could associate $Nd^{\bullet}_{Ca}$ to establish associated centre $Nd^{\bullet}_{Ca}Li'_{Ca}$ to neutralize the charge. The principle of charge balance is expressed in Eq. (2) and Eq. (3), the maxima at 4% Li^+-doping can be ascribed to this mechanism. But too much Li^+-doping could trap the CaF_2 NPs into a situation where defect centers Li'_{Ca} were too easy to establish so that charge balance (Eq. (3)) was broken up and the luminescence would be declined. From Fig. 4B, we can see the fluorescence intensity declined consistently versus Li^+ doping from 4% to 20%. There wasn't a great luminescence threshold until Li^+ doping density increased to 30%, where transformation can be ascribed to improved crystallinity and increased grain size [38,39], Fig. 3A-E could well prove this conclusion. However, continually increasing Li^+ doping would shrink grain size and cause reduced crystallinity (Fig. 3A and Fig. 3D-E), so the 50%

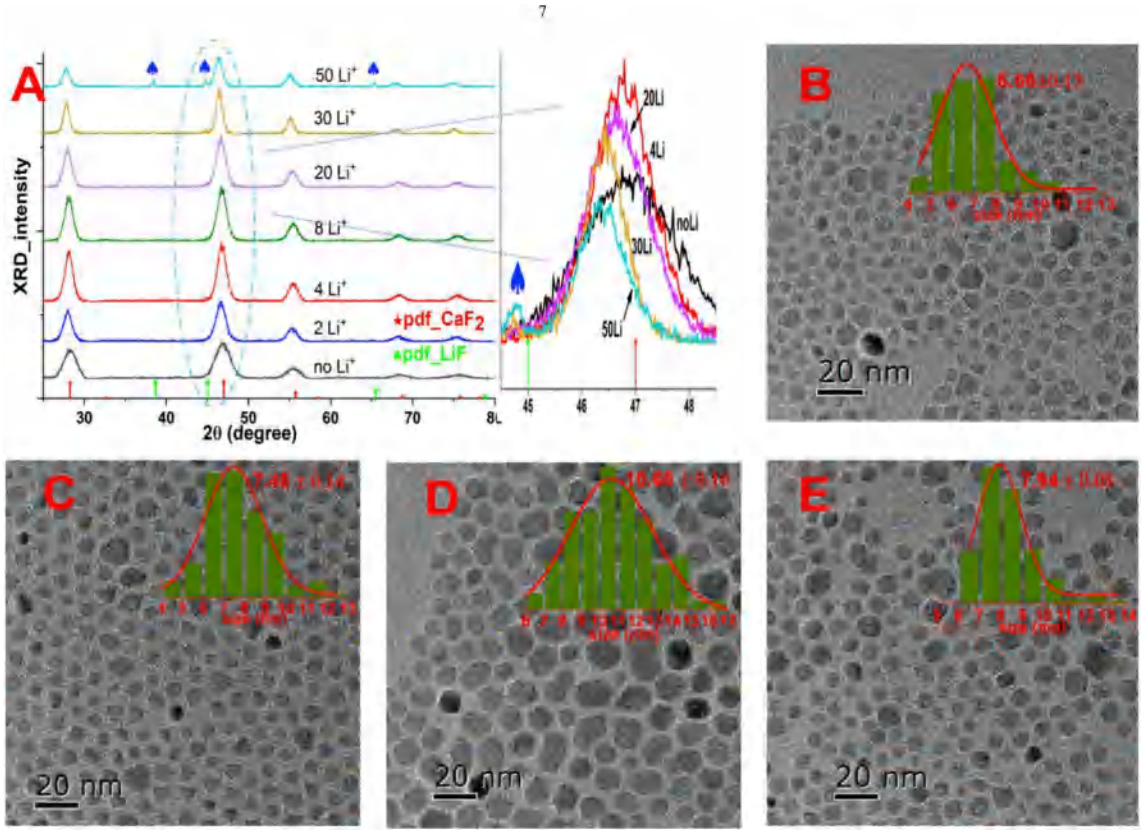

Fig. 3. (A).The X-ray diffraction spectra for varied CaF_2: xLi, 6Nd(mol%) NPs (the blue leaves signal the appearance of LiF peak, the right is the zoom for the blue dotted part ranged from 44° to 49°). The TEM images for various CaF_2: xLi, 6Nd(mol%) NPs with 20 nm scale bar, 4% Li^+-doping **(B),** 20% Li^+-doping**(C),** 30% Li^+-doping**(D),** 50% Li^+-doping**(E).** (For interpretation of the references to colour in this figure legend, the reader is referred to the Web version of this article.)

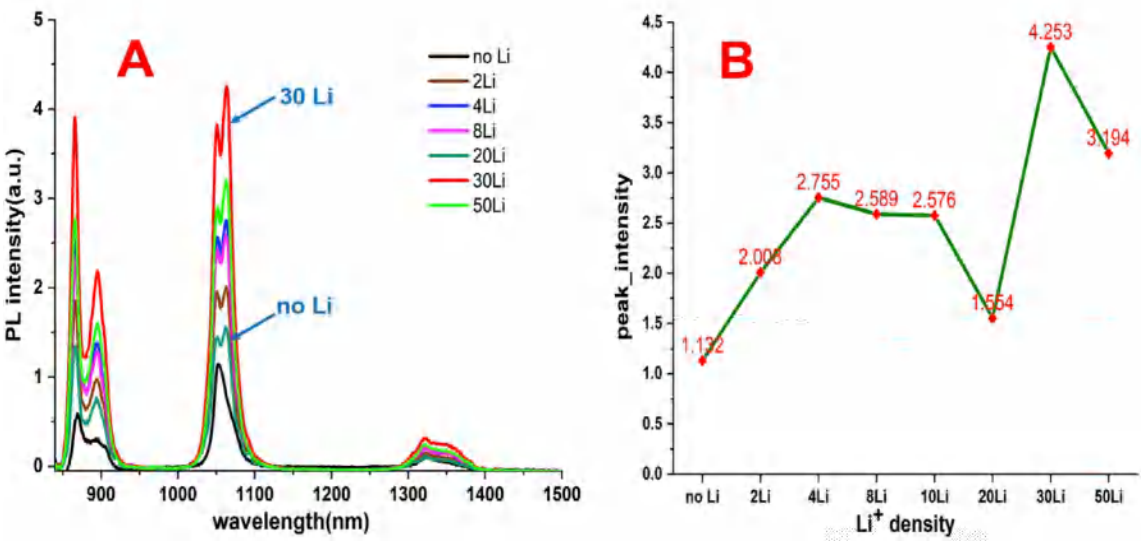

Fig. 4. (A) Emission spectra of CaF_2: xLi, 6Nd(mol%) NPs illustrating the intensity varying with Li^+ concentration excited by an 808 nm laser. **(B)** The strongest photoluminescence intensity for peak at 1.06 μm versus Li^+ density.

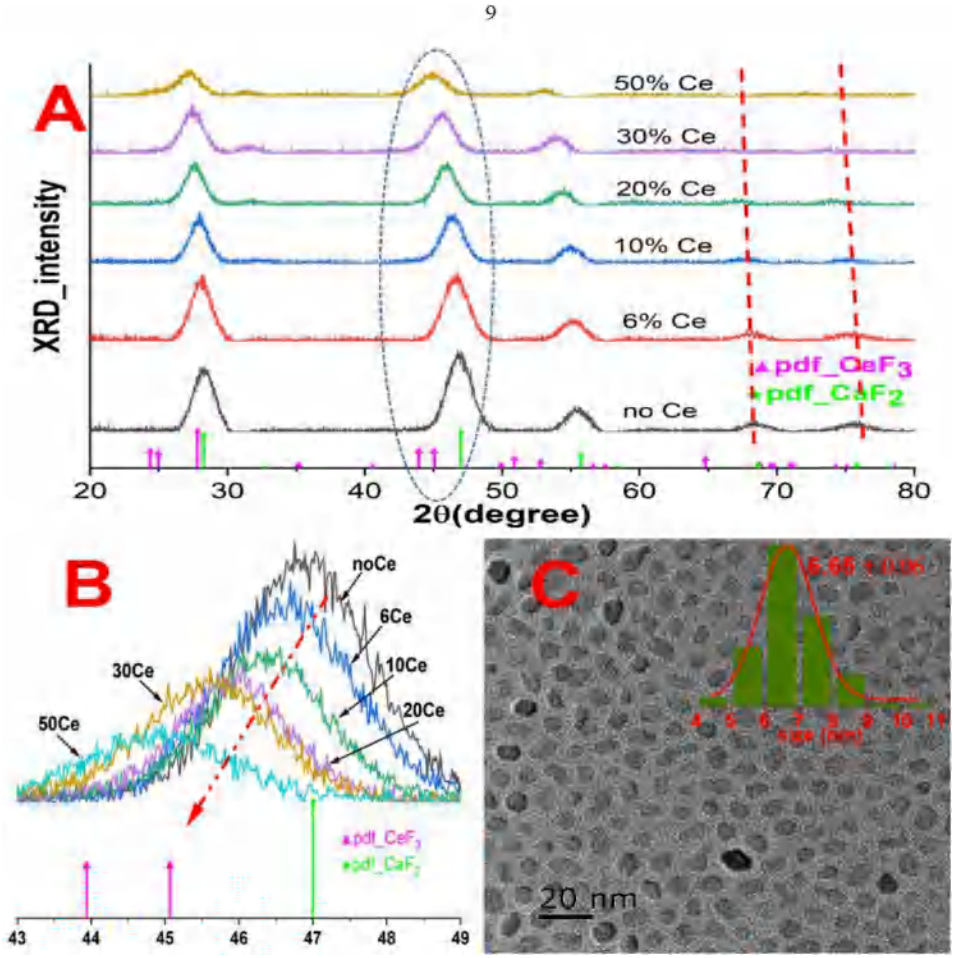

Fig. 5. (A) The X-ray diffraction spectra for various CaF_2: xCe,6Nd (mol%) NPs (the red dotted line showed the disappearance of diffraction peaks of CaF_2 at 68° and 75°), **(B)**The enlarged XRD spectra for the blue ellipse dotted part ranged from 43° to 49°in the **(A)**. **(C)** TEM image for CaF_2:20Ce,6Nd NPs with an average size 6.65 nm. (For interpretation of the references to colour in this figure legend, the reader is referred to the Web version of this article.)

Li^{+}-doping NPs' intensity decreased.

3.4. Ce^{3+} doping characterization and fluorescent performances

Finally, we exploited Ce^{3+} doping effect to CaF_2:6Nd(mol%) NPs Ce^{3+} doping as it has distinguished charge and diameter from Li^{+}, moreover it is useful to weaken the up-conversion and inversely increase the down-conversion, so a series of CaF_2:6Nd,xCe(mol%) NPs with different content of Ce^{3+} were synthesized. The actual amount of Ce^{3+} was characterized by energy dispersive spectrum (EDS). Taken CaF_2: 30Ce,6Nd(mol%) as example, the precursor concentration is 30%,EDS gave a (30 ± 0.5)% value, which accords well the precursor content ((Fig. S6C). Fig. 5 showed XRD spectra and TEM image for CaF_2:6Nd,xCe (mol%) NPs demonstrated their phase transformation and size evolution. In Fig. 5A and Fig. 5B, with Ce^{3+}-doping density increasing, the main diffraction peaks at 28°, 47°, 55° moved to smaller angle gradually (especially, the angle CaF_2: 30Ce,6Nd mol(%) at peak 47° downshifted up to 2.11° compared with CaF_2:6Nd(mol%), Fig. S6A), along with the diminishment of peaks at 68° and 75° bit-by-bit (red dotted line), and also together with the peak intensity ratio elevation at 28° and 47° (Fig. S6B). All these suggest that XRD diffraction peaks for highly Ce^{3+}-doping NPs has greatly disturbed the CaF_2 lattice and become coordinated with the peak for CeF_3 lattice much more. TEM image of CaF_2: 20Ce,6Nd(mol%) NPs in Fig. 5C exhibited that the NPs had an average dimeter of 6.65 nm, and the NPs were mainly hexagonal shape (TEM images for CaF_2: 10Ce,6Nd (mol%) and CaF_2: 30Ce,6Nd(mol%) were shown in Fig. S6), which varied greatly with that before Ce^{3+} doping (CaF_2:6Nd(mol%) NPs with 4.6 nm size and cubic shape) (Fig. 1E).

Then the photo luminescence behavior of CaF_2:6Nd,xCe(mol%) NPs upon 808 nm excitation was also investigated. The photo luminescence spectra were given in Fig. 6A. As can be seen, the main emission peaks at 0.9 μm, 1.06 μm and 1.32 μm obeyed a monotonically increase rule. Especially, the peak at 1.06 μm for CaF_2: 50Ce,6Nd(mol%) NPs was enhanced for 10.9 times than that of CaF_2:6Nd (mol%) NPs (Fig. 6B), and 2.9 times for the CaF_2: 30Li,6Nd(mol%) NPs. We inferred the enhanced fluorescence resulted from two reasons. The first reason is the greatly changed crystal symmetry and local crystal field around Nd^{3+} ions. The second reason is the dissociation of clusters upon Ce^{3+} doping. On the one hand, compared with that of Li-doping case, the main XRD diffraction peaks for CaF_2: 50Ce,6Nd(mol%) NPs showed a 3 times higher angle change, larger FWHM (Fig. S5 and Fig. S6) and lower diffraction intensity (Figs. 3 and 5) than those of CaF_2: 30Li,6Nd(mol%), which indicated a larger change of crystallinity and the disorder extent upon Ce^{3+} doping. It could be interpreted as that with Ce^{3+} doping increasing, Ce^{3+} will substitute the lattice of Ca^{2+}, the NPs tend to transfer from cubic phase(CaF_2) to hexagonal phase(CeF_3). Meanwhile, due to the diameter and electric charge difference of Ce^{3+} and Ca^{2+}, this would greatly decrease the crystal symmetry and local crystal field around Nd^{3+} ions [40,41] in CaF_2: xCe,6Nd (mol%) NPs, and hence change their fluorescence. On the other hand, the NIR-II emission of Nd^{3+} is easy to be quenched because of the clustering of Nd^{3+}, which even occurred at a very rather low Nd^{3+} concentrations (in the order of 1 mol %) [42]. Due to cross-relaxation processes between adjacent Nd^{3+}, this would quench the $^4F_{3/2}$ emitting level and decrease the $^4F_{3/2}$ emission from Nd^{3+} greatly [43,44]. Our doping optimizations were under the basis of 6%Nd^{3+} doped NPs, the quench had great effects on fluorescence. When Ce^{3+} and Nd^{3+} were co-doped into the CaF_2 NPs, for their similar diameter (Ce^{3+} is 1.02 Å, Nd^{3+} is 0.98 Å) and lattice match (both CeF_3 and NdF_3 belong to hexagonal system), Nd^{3+} would enter into Ce^{3+} site and well distributed in CaF_2: xCe,6Nd(mol%) NPs. And the Nd^{3+}-Nd^{3+} cluster will be broken and free Nd^{3+} will increase, hence the fluorescence will increase with it. The mechanism of Ce^{3+} doping to increase PL intensity is very effective, which can be further tested by Ce^{3+}/Li^{+} co-doped experiment that the Ce^{3+} has a dominate effect on the PL intensity (Fig. S7 depicted the XRD spectra and S8 displayed the PL behavior of Ce^{3+}, Li^{+} co-doped CaF_2:xLi, yCe,6Nd(mol%) NPs). So Ce^{3+}-doping is promising to greatly elevate the down-conversion transition and NIR emission of CaF_2:Nd^{3+} NPs.

4. Conclusions

In summary, we found a new and convenient method to synthesize CaF_2:Nd^{3+} NPs by $Ca(OH)_2$ and NH_4F using coprecipitation method. Subsequently, by regulation of temperature, reaction time, concentration of the solute and stirring condition CaF_2:Nd^{3+} NPs with a size ranging from 2.2 to 4.6 nm could be synthesized. With the 4.6 nm NPs' synthetic condition as basis, we synthesized a series of Nd^{3+}-doped CaF_2: Nd^{3+} NPs and found CaF_2:6Nd (mol%) NPs displayed the strongest emission. Then we explored two mechanisms of material modifications by Li^{+} ions and Ce^{3+} ions doping: for Li^{+} doping, the main luminescent magnification was primarily caused by improved crystallinity and increased grain size. As for Ce^{3+}-doping, because of its properties (ion diameter, host lattice) are different between Ca^{2+} and accordance with Nd^{3+} comparing Li^{+} doped CaF_2:6Nd (mol%) NPs, the enhanced

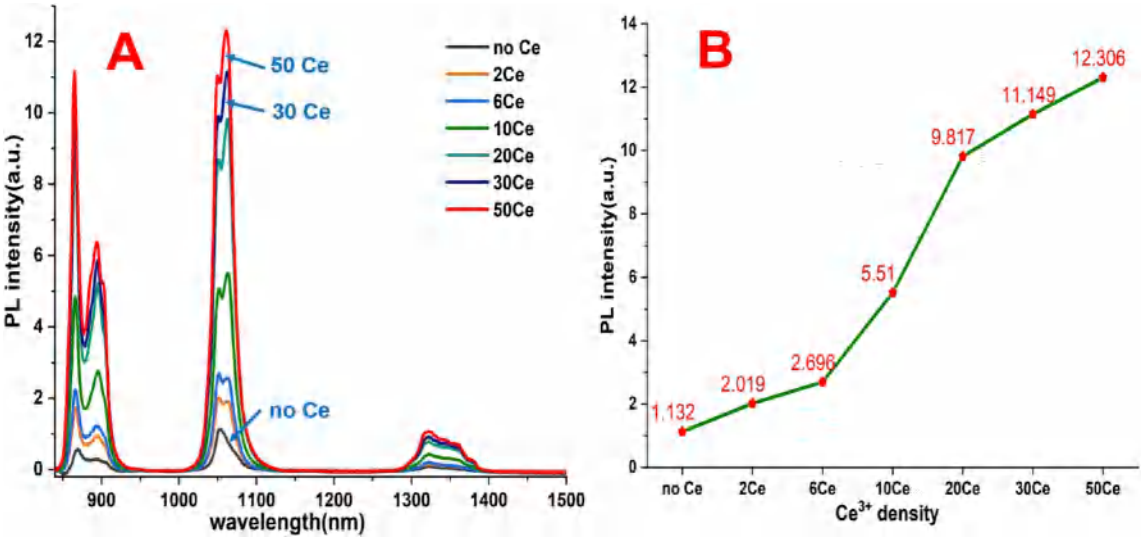

Fig. 6. (A) Emission spectra of CaF_2:6Nd,xCe(mol%) NPs depicted the intensity varying with Ce^{3+} concentration under 808 nm excitation. (B) The strongest photoluminescence intensity for peak at 1.06 μm versus Ce^{3+} density.

emission mainly resulted from the lowered crystal symmetry, changed local crystal field and broken Nd^{3+}-Nd^{3+}clusters. 50% Ce^{3+} doped NPs exhibited a more efficient fluorescence, the emission intensity at the peak of 1.06 μm is 10.9 times and 2.9 times stronger than that of non-doped NPs and Li-doped NPs separately, and obviously more prospective in NIR applications.

Declaration of competing interest

The authors declare that they have no conflict of interest.

Acknowledgments

We thank the research programs from National Key R&D Program of China (2016YFA0200800), the National Natural Science Foundation of China (Grant Nos. 61831021, 61771460 and 51641307), and we acknowledge a grant from the Youth Innovation Promotion Association CAS (2015190).

Appendix A. Supplementary data

Supplementary data to this article can be found online at https://doi.org/10.1016/j.dyepig.2019.108129.

References

[1] Chatterjee DK, Gnanasammandhan MK, Zhang Y. Small 2010;6:2781–95.
[2] Li ZQ, Zhang Y, Jiang S. Adv Mater 2008;20:4765–9.
[3] Diao S, Hong G, Antaris AL, Blackburn JL, Cheng K, Cheng Z, Dai H. Nano Res 2015;8:3027.
[4] Hong G, Antaris AL, Dai H. Nat. Biomed. Eng. 2017;1. 0010.
[5] Kenry, Duan YK, Liu B. Adv Mater 2018;30. 180 2394.
[6] van Saders B, Al-Baroudi L, Tan MC, Riman RE. Opt Mater Express 2013;3(5):566–73.
[7] Dong H, Sun LD, Yan CH. Chem Soc Rev 2015;44:1608–34.
[8] Jiang X, Cao C, Feng W, Li F. J Mater Chem B 2016;4:87.
[9] (a) Bensalah A, Mortier M, Patriarche G, Gredin P, Vivien DJ. Solid State Chem 2006;179:2636.(b) Sun X, Li Y. Chem Commun 2003;34:1768.
[10] Pedroni M, Piccinelli F, Passuello T, Giarola M, Mariotto G, Polizzi S, Bettinellia M, Speghini A. Nanoscale 2011;3:1456.
[11] Wang G, Peng Q, Li Y. J Am Chem Soc 2009;131(40):14200–1.
[12] Shannon RD, Prewitt CT. Acta Crystallogr Sect B: Struct Crystallogr Cryst Chem 1969;25:925.
[13] Ito M, Goutadier C, Guyot Y, et al. J Phys: Condens Matter 2004;16:1501–21.
[14] Chang HJ, Xie J, Zhao BZ, Liu B, Xu S, Ren Na, Xie X, Huang L, Huang W. Nanomaterials 2015;5:1–25.
[15] Xu B, He H, Gu Z, Jin S, Ma Y, Zhai T. J Phys Chem C 2017;121:18280–7.
[16] Yu Z, Shi J, Li J, Li P, Zhang H. J Mater Chem B 2018;6:1238–43.
[17] Liu Y, Tu D, Zhu H, Chen X. Chem Soc Rev 2013;42:6924.
[18] Rinkel T, Nordmann J, Raj AN, Haase M. Nanoscale 2014;6:14523–30.
[19] Johnson NJJ, Oakden W, Stanisz GJ, Scott Prosser R, van Veggel FCJM. Chem Mater 2011;23:3714–22.
[20] Huang Q, Ye W, Jiao X, Yu L, Liu Y, Liu X. J Alloy Comp 2018;763:216–22.
[21] Cui Y, Meng Q, Lü S, Sun W. Chemistry Select 2019;4(14):4316–23.
[22] Hong AR, Kim SY, Cho SH, Lee K, Jang HS. Dyes Pigments 2017;139(Complete):831–8.
[23] Wang F, Han Y, Lim C, Lu Y, Wang J, Xu J, Chen H, Zhang C, Hong M, Liu X. Nature 2010;463(7284):1061–5.
[24] Balavandy SK, Shameli K, Biak DRBA, Abidin ZZ. Chem Cent J 2014;8(1):11.
[25] Nie KB, Wang XJ, Wu K, Xu L, Zheng MY, Hu XS. J Alloy Comp 2011;509:8664–9.
[26] Jeong JH, Yang HK, Moon BK, Bae JS, Yi SS, Choi H, Kim JH, Chung ST. Opt Mater 2006;28:693–7.
[27] Yi SS, Shim KS, Yang HK, Moon BK, Choi BC, Jeong JH, Kim JH, Bae JS. Appl Phys Mater Sci Process 2007;87:667.
[28] Yu X, Xu X, Zhou C, Tang J, Peng X, Yang S. MaterRes Bull 2006;41:1578–83.
[29] Fan T, Zhang Q, Jiang Z, Yue J, Zhang M. J Opt 2011;13. 015001–015004.
[30] Zhong Y, Ma Z, Zhu S, Yue J, Zhang M, Antaris AL, Yuan J, Cui R, Wan H, Zhou Y, Wang W, Huang NF, Luo J, Hu Z, Dai H. Nat Commun 2017;8:737.
[31] Sawala NS, Omanwar SK. Infrared Phys Technol 2016;77:480–4.
[32] Li X, Shen D, Yang J, Yao C, Che R, Zhang F, Zhao D. Chem Mater 2013;25:106–12.
[33] Zhou J, Liu Q, Feng W, Sun Y, Li F. Chem Rev 2015;115(1):395–465.
[34] Thanh N, Maclean N, Mahiddine S. Chem Rev 2014;114:7610–30.
[35] Fan T, Lü J, Huang Y, Li G. Micro & Nano Lett 2018;13:393–6.
[36] Yuan D, Li W, Mei B, Song J. J Nanosci Nanotechnol 2015;15:9741–5.
[37] Du Q, Zhou G, Zhou J, Zhou H. J Lumin 2013;137:83–7.
[38] Gu F, Li C, Cao H, Shao W, Hu Y, Chen J, Chen A. J Alloy Comp 2008;453:361–5.
[39] Ma Q, Zhou Y, Zhang A, Lu M, Zhou G, Li C. Solid State Sci 2009;11:1124–30.
[40] Luo L, Liu HB, Yao LL, Dong GS, Zhang W, Wang YH, Qiu ZR, Chen J. J Nanosci Nanotechnol 2016;16:626–31.
[41] Klier DT, Kumke MU. J Phys Chem C 2015;119:3363–73.
[42] Voron'Ko YK, Osiko VV, Prokhorov AM, Shcherbakov IA. J Exp Theor Phys 1971;33:37–55.
[43] Danielmeyer HG, Blatte M, Balmer P. Appl Phys 1973;1:269–74.
[44] Quintanilla M, Zhang Yang, Liz-Marzań LM. Chem Mater 2018;30:2819–28.